Magma Chamber Process of Post-collisional Magmatism: Insight from Textural and Elemental Characteristics of Plagioclase from the Tatun Volcanic Group, Northern Taiwan Volcanic Zone

1922—2022

ZHANG Xia[1], GUO Kun[1, 2, *], ZHANG Yu[1], LAI Zhiqing[3,*], JIANG Shulong[4], JIANG Wenpeng[4] and LI Jingbo[4]

[1] *Pilot National Laboratory for Marine Science and Technology (Qingdao), Qingdao, Shandong 266237, China*
[2] *Key Laboratory of Marine Geology and Environment, Institute of Oceanology, Chinese Academy of Sciences, Qingdao, Shandong 266071, China*
[3] *Key Lab of Submarine Geosciences and Prospecting Techniques, MOE and College of Marine Geosciences, Ocean University of China, Qingdao, Shandong 266100, China*
[4] *Shandong Province Nuclear Industry Geological Group 248, Qingdao, Shandong 266000, China*

Abstract: The Taiwan mountain belt, one of the youngest orogenies in the world, is caused by the collision of the Luzon arc with the Eurasian margin, which leads to post-collisional extension and magmatism in the Northern Taiwan Volcanic Zone (NTVZ). The magma chamber process in this region has not previously been elucidated in detail. In this paper, the textural and compositional features of plagioclase phenocrysts in basalt from the Tatun Volcanic Group (TTVG) were studied to restrict the dynamics of magma system. Results show that the magma melts in TTVG are mainly sourced from the underlying MORB-like mantle wedge but influenced by incorporation of subduction components, causing the elevated Sr/Y and Ba/Y ratios in magma melts. The subduction components are mainly transported in the form of sediment melt. The plagioclase phenocrysts in the TTVG volcanic rocks are generally coarsely core-sieved with a clear rim. The An contents in the rims of plagioclase are much lower than those of cores, and elevated FeO concentrations are detected in the plagioclase rims. We propose there exists a double-layer magma chamber in this region. The core of the plagioclase was crystalized in the deeper quiescent magma chamber (~21 km), which was subsequently partially dissolved during the ascent of magma melt under H_2O-undersaturated condition, forming the typical coarsely sieved texture and synneusis. When this crystal-rich melt migrates into the shallower chamber, water saturation is reached and more sodic plagioclase formed as the rim of phenocryst. Due to the considerably higher fO_2 in the shallow chamber than in the deeper one, and the distribution of Fe between plagioclase and melt positively correlates with fO_2, the FeO content in the plagioclase rim elevates in conjunction with increasing fO_2.

Key words: plagioclase, textural and compositional features, dynamics of magma system, Tatun Volcanic Group

Citation: Zhang et al., 2022. Magma Chamber Process of Post-collisional Magmatism: Insight from Textural and Elemental Characteristics of Plagioclase from the Tatun Volcanic Group, Northern Taiwan Volcanic Zone. Acta Geologica Sinica (English Edition), 96(5): 1587–1599. DOI: 10.1111/1755-6724.14810

1 Introduction

Collisional orogenic belts are typically marked by changes in the composition of the associated magmatism, and the subduction-related features resulted from metasomatism by slab derived fluids of the mantle lithosphere before collision (Pearce et al., 1990; Turner et al., 1996; Wang et al., 2004; Huang et al., 2021; Li et al., 2022; Zhang et al., 2022). Post-collisional magmatism, one of the common features of many orogens around the world responsible for the cessation of collision and onset of extensional collapse (Wang et al., 2004; Meshram et al., 2022), shows extension tectonic characteristics (Rateb et al., 2017), and reveals changes in magma source and magma chamber process with orogen (Liu et al., 2014; Wang and Zhang, 2022). Many important research achievements about post-collisional magmatism have been obtained, such as the composition of magma and mantle source reflected by the elemental and isotopic characteristics of volcanic rocks (Dai et al., 2016; Kong et al., 2020), the asthenosphere upwelling and mantle melting (Laurent et al., 2014; Zheng et al., 2015), the interaction between upper mantle and lower crust (Dong et al., 2011; Zhao et al., 2011; Hébert et al., 2014; Hu et al., 2016), the various differentiation of physical chemistry during the process of magmatic rock reforming (Zheng et al., 2011; Gao et al., 2014; Zhao et al., 2015), the structural control on magmatism (Chung et al., 2005; Zhao et al., 2013; Seghedi et al., 2019). All in all, the above-mentioned scientific results are obtained mainly by the

* Corresponding author. E-mail: kguo@qnlm.ac; laizhiqing@ouc.edu.cn

whole rock geochemistry. As we all know, rock is a product of crystallization differentiation of magma in a magma chamber or/and aisle (e.g., Manikyamba et al., 2022). Hence it could not represent the composition of primary magma. Whereas minerals such as plagioclase make a crucial contribution to the reconstruction of the history of crystallization differentiation processes in magma chambers. However, the researches about the kinematics and process of magma chamber in post-collisional areas are less, which influence the evolution, rise and extrusion of magma. The magma chamber process of post-collisional areas research is beneficial to better understand the variation of geochemical composition of magma in the whole process from collision to cessation.

Taiwan Island, which is located along the convergent boundary between the Philippine Sea Plate and the Eurasian Plate (Fig. 1), was generated by the subduction of the South China Sea (SCS) and the subsequent arc-continent collision between the South China continental margin and the north Luzon arc (Tian et al., 2019). The post-collisional extension in the northern Taiwan mountain belt (NTMB) resulted in the magmatism of the Northern Taiwan Volcanic Zone (NTVZ). The Tatun Volcanic Group (TTVG) is located in the west end of NTVZ, which is an ideal area to research magma chamber process in post-collisional areas. Plagioclase is a common mineral in volcanic rocks, which can crystalize over a wide range of temperatures and persist as a crystallizing phase throughout cooling and eruption (Viccaro et al., 2010). Due to the CaAl-NaSi diffusion exchange within the plagioclase crystal is extremely slow, the compositional and textural zoning patterns developed during the primary growth are generally preserved (Grove et al., 1984; Lai et al., 2018; Chen et al., 2020). Many studies have demonstrated that the texture and chemical zoning patterns of plagioclase may be an efficient tool for confining the dynamics of magmatic processes, due to its high sensitivity to changes in physical-chemical conditions of magma system (Blundy and Shimizu, 1991; Stimac and Pearce, 1992; Singer et al., 1995; Tepley et al., 2000; Humphreys et al., 2006; Smith et al., 2009; Viccaro et al., 2010; 2012; Renjith et al., 2014; Lai et al., 2016). Hence, in this study, using textural and compositional element features of plagioclase from TTVG basalts, we aim to investigate the dynamics of magma system and the influence of subducted component.

2 Geological Setting

The Northern Taiwan Volcanic Zone (NTVZ), located near the southern end of the Okinawa Trough, consists of onshore volcanic fields and several offshore volcanoes (Fig. 1). The NTVZ volcanic rocks are dominated by andesites with calc-alkaline geochemical characteristics, similar to those of convergent-margin lavas (Gill, 1981). Thus, these volcanos were considered as part of the Ryukyu Arc in the past (Chung et al., 1995; Teng et al., 1996). More recently, Chen et al. (1997) and Wang et al. (1999, 2004) propose that the NTVZ resulted from the post-collisional extension related to the late Pliocene

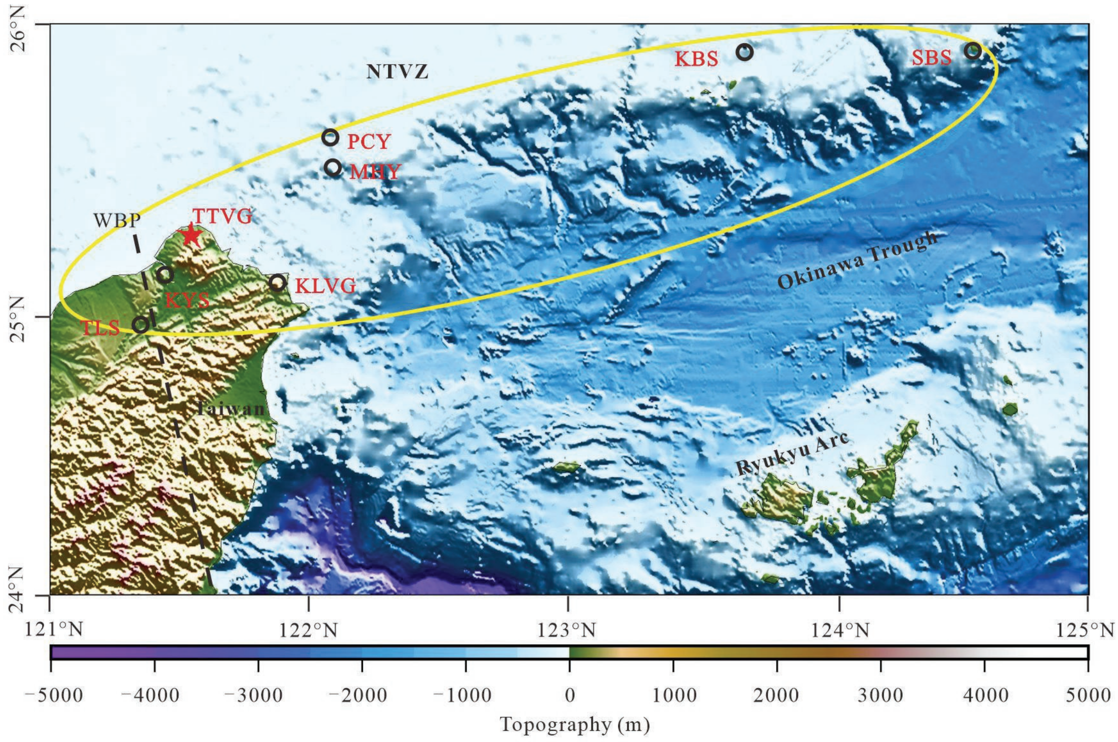

Fig. 1. Bathymetric map of the Northern Taiwan Volcanic Zone (NTVZ).
The sampling location is marked with the red star and the black circles represent the major volcanos in the NTVZ. WPB indicates the western boundary of the subducted Philippine Plate. TLS: Tslingshan, KYS: Kyanyinshan, TTVG: Tatun Volcanic Group, KLVG: Keelung Volcanic Group, PCY: Pengchiayui, MHY: Mienhuayui, KBS: Kobisho, SBS: Sekibisho.

orogenic collapse of the Northern Taiwan Mountain Belt (2.8–0.2 Ma). Previous researches have demonstrated that the magma sources in this region are complicated, which may encompass the asthenosphere and metasomatized subcontinental lithospheric mantle (Wang et al., 2004; Pi et al., 2016). These two components are represented by the 2.6 Ma Mienhuayu high-Mg basaltic andesites and the 0.2 Ma Tsaolingshan (TLS) high-Mg potassic lavas, respectively (Wang et al., 2004).

The Tatun Volcanic Group (TTVG), located in the northernmost of Taiwan Island (Fig. 1) and above the subducted western Philippine Plate, is one of the onshore volcanic fields in the NTVZ. Sr-Nd isotope ratios of the TTVG volcanic rocks ($^{87}Sr/^{86}Sr \approx 0.70428$–$0.70469$; $^{143}Nd/^{144}Nd \approx 0.51268$–$0.51280$) indicate that the magma source of TTVG is from the upwelling higher-degree asthenospheric melts were generated with less contamination by the overlying metasomatized subcontinental lithospheric mantle (Wang et al., 2004). Therefore, the TTVG basaltic volcanic rock is an ideal sample to research the dynamic of magma system from asthenospheric mantle in the background of post-collisional and subduction.

3 Samples and Analytical Methods

The volcanic rock samples (HRS-1 and HRS-2) studied in this paper were collected from the TTVG, one of the onshore volcanic fields in the NTVZ. Both of the samples are basalts and the phenocryst assemblage is composed of plagioclase, pyroxene and olivine. The sampling locations are shown in the Fig. 1. The volcanic rock samples were ultrasonically cleaned in ultra-pure water for three times firstly. Then, the dried samples were cut into thin sections and double polished for electron probe micro analysis (EPMA) and laser ablation inductively coupled plasma mass spectrometry (LA-ICP-MS) determination.

3.1 EPMA analysis

Several representative plagioclase phenocrysts were chosen for crosscut analyses by EMPA at Key Laboratory of Submarine Geosciences and Prospecting Techniques, Ministry of Education, Ocean University of China, Qingdao, China. Analytical conditions were acceleration voltage of 15 kV, a beam current of 20 nA, a spot diameter of 5 μm. The standards used in these analyses were albite for Na and Al; diopside for Mg, Si and Ca; sanidine for K; rutile for Ti; and almandine for Fe. The precision of the major element analyses was better than 1%, and that of the minor element analyses was better than 5%.

3.2 LA-ICP-MS analysis

Major elements and trace elements of Pl megacrysts were analyzed in thin sections and laser targets using LA-ICP-MS in Institute of Oceanology, Chinese Academy of Sciences. Laser sampling was performed using a Photon Machines Excite 193 nm excimer Ar-F laser system, and an Agilent 7900a ICP-MS instrument was used to acquire ion-signal intensities. Each analysis includes 20 seconds background acquisition (gas blank) followed by 50 seconds data acquisition. The samples were analyzed using a 40 μm spot and 7.42 J/cm^2 energy density at a repetition rate of 6 Hz. BCR-2G, BHVO-2G and BIR-1G are used as external standards for calibration. Every eight sample analyses were followed by two analyses of GSE-1G. All of the test data were processed offline using the ICPMSDataCal software version 11.8 (Liu et al., 2010). The measured values of the reference materials were in satisfactory agreement with the recommended values. For most trace elements, the analytical accuracy and precision were better than 10%.

4 Results

4.1 Micro-textures and compositional profiles of plagioclase

The micro-texture and crosscut chemical compositions of typical plagioclase phenocrysts were analyzed by EPMA. Plagioclase phenocrysts in sample HRS-1 and HRS-2 are generally euhedral with homogeneous cores and thin rims (Supp. Table 1). The cores of the plagioclase phenocrysts are generally coarsely–sieved due to the strong dissolution. In several plagioclase cores, weak oscillatory zoning was developed. Besides, several synneusis were also observed in our samples and the plagioclase phenocrysts that formed the synneusis share the same rim. Calculated An contents of the plagioclase phenocrysts show large variations (An 49–92, Supp. Table 1). In general, the cores of the plagioclase have high An contents (An 78–92), which are similar to the analyses results of LA-ICP-MS (An 71–86, see section 4.2). While the An contents in the rims of plagioclase are much lower accompanied by the increase of FeO contents (Supp. Table 1). In the An–Ab–Or compositions of plagioclase phenocrysts (Fig. 2), the cores and rims of plagioclase fall in the different range, plagioclase cores are categorized as bytownite and anorthite, whereas plagioclase rims are identified as labradorite.

The $K_D(Ab–An)^{pl–liq}$ values and thermobarometry calculations were conducted according to the model proposed by Putirka (2008) in order to discuss the

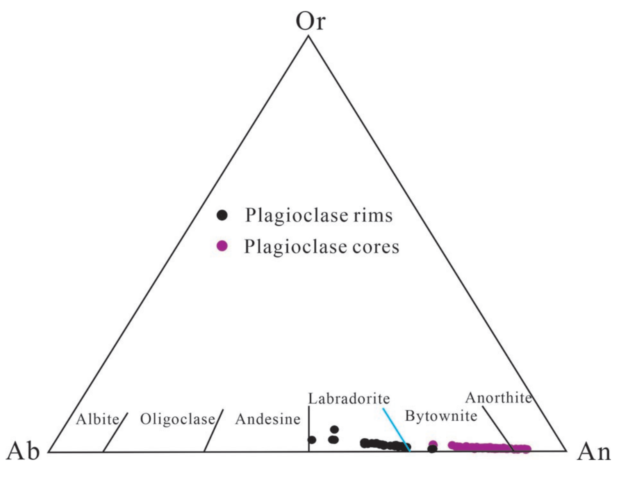

Fig. 2. An–Ab–Or compositions of plagioclase phenocrysts from the TTVG basalt.
The plagioclase cores mainly fall in the bytownite, whereas the plagioclase rims plots as labradorite.

crystallization temperature and pressure of the plagioclase, and the results are shown in Table 1. The calculated crystallization temperatures and pressures of the representative plagioclase cores are about 1245°C and 8 kbar, respectively. While the rims and several cores of the plagioclase are out of equilibrium with the melt, thus, the calculations were not conducted (see detail in section 5.3).

4.2 LA-ICP-MS analysis results

Thirty typical plagioclase phenocrysts from HRS-1 and HRS-2 were analyzed by LA-ICP-MS, results show that the chemical compositions of plagioclase in these two samples are quite similar (Table 2). Calculated An contents range from 71 to 86, and the lower An contents, as determined by EPMA, were not detected, which is because the LA-ICP-MS analysis were conducted in the plagioclase core, while the low An contents are entirely concentrated in the plagioclase rim. The chondrite-normalized REE patterns of the NTVZ plagioclase are uniformly LREE enriched and show strong positive Eu anomalies (Fig. 3). The contents of La, Sr, Ba and Y in primary melt were calculated in order to discuss the magma source and subduction component influence (see detail in section 5.1). Calculated results are shown in the Table 3.

5 Discussion

5.1 Magma source and subduction influence

The magma source of TTVG has been the subject of much debate. Wang et al. (2004) propose that the magma source of TTVG is from the upwelling higher-degree asthenospheric melts were generated with less contamination by the overlying metasomatized subcontinental lithospheric mantle. While B isotope research of volcanic rocks form TTVG indicates that the magma is mainly sourced from the underlying MORB-like mantle wedge with a little proportion of incorporated subduction components (Pi et al., 2016). In order to clarify the magma source composition in TTVG from the viewpoint of plagioclase, we calculated the trace element concentrations in magma melt from which the plagioclase crystalized according to the following equation:

$$C_M = C_{Pl}/D$$

where D is the partition coefficient, C_{Pl} and C_M are element concentrations in plagioclase and primary melt respectively. Due to the LA-ICP-MS analysis were conducted in the plagioclase cores and their compositions are in equilibrium with the magma melt (see in section 5.3), the D values can be calculated using the method of Sun et al. (2017) and the calculated trace element contents in parental melt compositions are shown in the Table 3.

In the Fig. 4, the TTVG magma melts are plotted near the MORB line but show apparently higher Sr/Y and Ba/Y ratios, which indicates that the magma melts in the TTVG are mainly sourced from the MORB-like mantle but influenced by the incorporation of Sr and Ba from other sources. Crustal contamination and incorporation of subduction components may be the probable reasons for the elevated Sr/Y and Ba/Y ratios. However, previous researches have demonstrated that the crustal

Table 1 Thermobarometry calculations results of the representative TTVG plagioclase

Sample ID	K_D	T (°C)	P (kbar)	Sample ID	K_D	T (°C)	P (kbar)
HRS-1 Pl-core	0.20	1245	8.1	HRS-1 Pl-core	0.17	1244	7.9
HRS-1 Pl-core	0.20	1244	8.1	HRS-1 Pl-core	0.20	1244	8.1
HRS-1 Pl-core	0.18	1244	7.9	HRS-1 Pl-core	0.20	1244	8.0
HRS-1 Pl-core	0.20	1244	8.0	HRS-1 Pl-core	0.21	1244	8.1
HRS-1 Pl-core	0.17	1244	7.9	HRS-1 Pl-core	0.17	1244	7.9
HRS-1 Pl-core	0.16	1245	7.8	HRS-1 Pl-core	0.15	-	-
HRS-1 Pl-core	0.15	-	-	HRS-1 Pl-core	0.16	1245	7.8
HRS-1 Pl-core	0.17	1244	7.9	HRS-1 Pl-core	0.20	1244	8.1
HRS-1 Pl-core	0.16	1245	7.8	HRS-1 Pl-core	0.25	1243	8.5
HRS-1 Pl-core	0.16	1245	7.9	HRS-1 Pl-core	0.16	1245	7.8
HRS-1 Pl-core	0.16	1245	7.8	HRS-1 Pl-core	0.12	-	-
HRS-1 Pl-core	0.15	-	-	HRS-1 Pl-core	0.12	-	-
HRS-1 Pl-core	0.20	1245	8.1	HRS-1 Pl-core	0.08	-	-
HRS-1 Pl-core	0.10	-	-	HRS-1 Pl-core	0.10	-	-
HRS-1 Pl-core	0.15	-	-	HRS-1 Pl-core	0.12	-	-
HRS-1 Pl-core	0.08	-	-	HRS-1 Pl-core	0.11	-	-
HRS-1 Pl-core	0.08	-	-	HRS-1 Pl-core	0.12	-	-
HRS-1 Pl-core	0.12	-	-	HRS-1 Pl-core	0.09	-	-
HRS-1 Pl-core	0.14	-	-	HRS-1 Pl-core	0.12	-	-
HRS-1 Pl-core	0.13	-	-	HRS-1 Pl-core	0.11	-	-
HRS-1 Pl-core	0.09	-	-	HRS-1 Pl-core	0.10	-	-
HRS-1 Pl-core	0.18	1244	7.9	HRS-1 Pl-core	0.17	1244	7.9
HRS-1 Pl-core	0.14	-	-	HRS-1 Pl-core	0.14	-	-
HRS-1 Pl-core	0.15	-	-	HRS-1 Pl-core	0.17	1244	7.9
HRS-1 Pl-core	0.17	1244	7.9	HRS-1 Pl-core	0.18	1244	8.0
HRS-1 Pl-core	0.26	1243	8.7	HRS-1 Pl-core	0.20	1244	8.1
HRS-1 Pl-rim	0.54	-	-	HRS-1 Pl-rim	0.48	-	-
HRS-1 Pl-rim	0.53	-	-	HRS-1 Pl-rim	0.51	-	-
HRS-1 Pl-rim	0.51	-	-	HRS-1 Pl-rim	0.42	-	-
HRS-1 Pl-rim	0.59	-	-	HRS-1 Pl-rim	0.32	-	-
HRS-1 Pl-rim	0.76	-	-	HRS-1 Pl-rim	0.51	-	-
HRS-1 Pl-rim	0.76	-	-	HRS-1 Pl-rim	0.58	-	-
HRS-1 Pl-rim	0.56	-	-	HRS-1 Pl-rim	0.48	-	-
HRS-1 Pl-rim	0.46	-	-	HRS-2-Pl-core	0.20	1244	8.1
HRS-2-Pl-core	0.17	1245	7.9	HRS-2-Pl-core	0.17	1245	7.9
HRS-2-Pl-core	0.16	1245	7.8	HRS-2-Pl-core	0.14	-	-
HRS-2-Pl-core	0.15	-	-	HRS-2-Pl-core	0.14	-	-
HRS-2-Pl-core	0.14	-	-	HRS-2-Pl-core	0.16	1245	7.8
HRS-2-Pl-core	0.14	-	-	HRS-2-Pl-core	0.14	-	-
HRS-2-Pl-core	0.17	1245	7.9	HRS-2-Pl-core	0.15	-	-
HRS-2-Pl-core	0.19	1244	8.0	HRS-2-Pl-core	0.16	1245	7.8
HRS-2-Pl-core	0.14	-	-	HRS-2-Pl-core	0.15	-	-
HRS-2-Pl-core	0.19	1244	8.0	HRS-2-Pl-core	0.22	1244	8.2
HRS-2-Pl-core	0.18	1245	8.0	HRS-2-Pl-core	0.20	1244	8.1
HRS-2-Pl-core	0.18	1245	8.0	HRS-2-Pl-core	0.19	1244	8.0
HRS-2-Pl-core	0.14	-	-	HRS-2-Pl-core	0.16	1245	7.9
HRS-2-Pl-core	0.15	-	-	HRS-2-Pl-core	0.15	-	-
HRS-2-Pl-core	0.14	-	-	HRS-2-Pl-core	0.13	-	-
HRS-2-Pl-core	0.16	1245	7.8	HRS-2-Pl-core	0.10	-	-
HRS-2-Pl-core	0.14	-	-	HRS-2-Pl-core	0.15	-	-
HRS-2-Pl-core	0.17	1245	7.9	HRS-2-Pl-core	0.16	1245	7.8
HRS-2-Pl-core	0.22	1244	8.2	HRS-2-Pl-core	0.16	1245	7.8
HRS-2-Pl-core	0.16	1245	7.9	HRS-2-Pl-core	0.21	1244	8.2
HRS-2-Pl-core	0.20	1244	8.1	HRS-2-Pl-core	0.22	1244	8.2
HRS-2-Pl-core	0.22	1244	8.2	HRS-2-Pl-core	0.32	1242	9.2
HRS-2-Pl-core	0.24	1244	8.4	HRS-2-Pl-core	0.23	1244	8.3
HRS-2-Pl-core	0.20	1244	8.1	HRS-2-Pl-core	0.19	1244	8.0
HRS-2-Pl-core	0.19	1244	8.0	HRS-2-Pl-core	0.24	1244	8.4
HRS-2-Pl-core	0.17	1245	7.9	HRS-2-Pl-rim	0.32	1242	9.2
HRS-2-Pl-rim	0.42	-	-	HRS-2-Pl-rim	0.43	-	-
HRS-2-Pl-rim	0.42	-	-	HRS-2-Pl-rim	0.50	-	-
HRS-2-Pl-rim	0.50	-	-	HRS-2-Pl-rim	0.58	-	-
HRS-2-Pl-rim	0.54	-	-	HRS-2-Pl-rim	0.53	-	-
HRS-2-Pl-rim	0.44	-	-	HRS-2-Pl-rim	0.45	-	-
HRS-2-Pl-rim	0.43	-	-	HRS-2-Pl-rim	0.51	-	-
HRS-2-Pl-rim	0.43	-	-	HRS-2-Pl-rim	0.75	-	-
HRS-2-Pl-rim	0.45	-	-				

Note: "-" means the plagioclase is not equilibrium with the melt and thermobarometry calculations were not conducted.

Table 2 Representative analyses of TTVG plagioclase phenocrysts by LA-ICP-MS

ID	SiO_2	Al_2O_3	CaO	Na_2O	K_2O	Sr	Ba	La	Ce	Pr	Nd	Sm	Eu	Gd	An
	48.28	32.43	16.37	1.88	0.09	812	59.98	1.45	2.71	0.21	0.93	0.20	0.45	0.07	78
	49.90	31.53	15.55	1.95	0.11	866	79.69	1.77	2.84	0.32	1.31	0.16	0.40	0.11	76
	53.59	29.54	14.12	1.67	0.11	753	70.04	1.72	2.62	0.32	0.96	0.29	0.34	0.07	77
	47.96	32.75	16.45	1.80	0.09	863	69.00	1.59	2.71	0.33	1.12	0.17	0.35	0.08	79
	46.95	33.26	17.58	1.32	0.05	716	41.52	0.89	1.42	0.16	0.69	0.19	0.24	0.04	84
	52.18	30.89	14.84	1.21	0.05	654	38.46	1.38	2.01	0.24	0.93	0.16	0.28	0.09	83
	48.29	32.41	16.18	1.85	0.13	897	83.12	2.22	3.83	0.43	1.52	0.29	0.41	0.18	78
HRS-1	48.31	31.91	16.63	1.73	0.17	783	73.59	1.97	3.59	0.41	1.63	0.20	0.40	0.26	79
	47.29	33.00	17.67	1.18	0.04	779	43.41	1.11	1.68	0.21	0.58	0.20	0.30	0.04	86
	48.58	32.21	16.28	2.00	0.10	596	22.91	0.58	1.10	0.09	0.33	0.02	0.17	0.10	77
	56.37	27.58	12.91	2.13	0.15	775	92.74	1.65	2.88	0.25	1.33	0.29	0.45	0.07	71
	47.90	32.76	16.89	1.51	0.07	849	64.13	1.38	2.51	0.30	0.80	0.07	0.46	0.13	82
	52.10	29.28	14.66	1.75	0.28	720	102.65	1.71	3.38	0.38	1.98	0.57	0.32	0.30	76
	48.65	31.10	16.00	1.89	0.24	814	90.77	3.44	6.71	0.80	3.54	0.85	0.54	0.50	77
	48.23	32.58	16.24	1.94	0.09	931	76.94	1.64	2.77	0.28	1.26	0.07	0.51	0.10	77
	47.37	32.76	17.60	1.31	0.05	709	37.27	0.87	1.32	0.19	0.66	0.12	0.26	0.08	84
	47.99	32.76	16.65	1.59	0.06	731	41.95	1.02	1.70	0.20	0.72	0.02	0.25	0.10	81
	48.34	32.46	16.45	1.85	0.07	629	37.12	1.08	1.93	0.17	0.77	0.06	0.22	0.15	78
	47.41	33.09	17.12	1.41	0.07	745	42.90	1.68	3.09	0.37	1.33	0.16	0.29	0.12	83
	47.96	32.44	16.48	2.05	0.11	941	88.01	1.83	4.44	0.37	1.19	0.35	0.43	0.10	76
	47.36	33.37	17.26	1.15	0.05	732	40.16	0.87	1.47	0.18	0.69	0.10	0.23	0.02	86
	48.18	32.89	16.80	1.52	0.06	663	41.97	1.15	1.86	0.18	0.83	0.06	0.27	0.06	82
HRS-2	49.18	31.63	15.74	1.97	0.16	868	84.67	2.77	4.62	0.50	2.49	0.22	0.46	0.26	76
	48.16	33.55	15.27	1.67	0.19	604	74.29	2.16	3.27	0.38	1.70	0.29	0.37	0.39	78
	48.17	32.71	16.76	1.51	0.05	649	36.83	0.80	1.49	0.20	0.46	0.04	0.30	0.06	82
	48.39	32.30	16.28	1.81	0.12	672	46.65	1.77	3.67	0.38	1.60	0.28	0.49	0.31	78
	48.96	33.59	14.43	1.89	0.11	845	129.29	2.76	4.07	0.73	1.73	0.33	0.50	0.25	75
	47.87	33.12	16.27	1.78	0.08	919	73.60	1.60	2.85	0.32	0.99	0.12	0.41	0.11	79
	45.99	33.83	17.81	1.45	0.05	751	42.81	1.00	1.49	0.14	0.52	0.08	0.26	0.02	83
	46.61	33.85	16.87	1.74	0.08	903	64.63	1.55	2.54	0.27	1.22	0.14	0.45	0.03	80

Note: major element contents (%), trace element contents (ppm), An: anorthite content in mole percent.

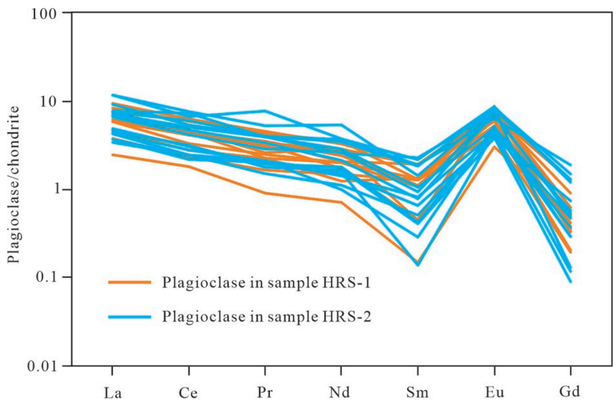

Fig. 3. Chondrite-normalized (Sun and Mcdonough, 1989) REE patterns of TTVG plagioclase.

Due to the contents of HREE are generally close to the detected limits of LA -ICP-MS, only LREE are shown here.

contamination in the TTVG was negligible (Wang et al., 2004; Pi et al., 2016), which exclude the influence of crust -derived Sr and Ba. Besides, crustal contamination is mainly occurred in the late stage of magmatism, while the plagioclase is crystalized in the early stage of magma fractionation, which is unlikely influenced by crustal contamination (Guo et al., 2016, 2018b; Chen et al., 2020). That is why plagioclase is commonly used to discuss the magma source information. Thus, we propose the melt calculated from the plagioclase compositions dose not record a crustal contamination influence. Sr and Ba have strong mobility during the slab subduction, thus, incorporation of subduction components in to the magma source will cause the elevated Sr/Y and Ba/Y ratios in magma melts (Guo et al., 2018a). This is consistent with the local tectonic setting that the westward propagation of Philippine Sea Plate under the northern Taiwan causing the incorporation of slab-derived component into the TTVG magma source (Wang et al., 2004). Therefore, we propose the subduction contribution to the magma source of TTVG is the major cause of elevated Sr/Y and Ba/Y ratios in the magma melts.

Then, one key remaining question is whether these subduction components are transported as aqueous fluid or sediment melt. Ba/La and La/Y ratios are good tracers for differentiating the slab-derived fluid and sediment melt components. This is because Ba, La and Y show very similar behavior during the mantle melting and fractional crystallization processes but are decoupled during subduction processes. Ba is mobile in low-temperature aqueous fluid, La is mobile in high-temperature sediment melts, while Y is immobile during subduction process (Guo et al., 2018a). In Ba/La vs La/Y diagrams (Fig. 5), the TTVG magma melts show near horizontal distribution, indicating that the subduction components are mainly incorporated into the magma source in the form of sediment melt with little proportion of slab-derived aqueous fluid. This conclusion is same as the contribution of subduction components for southern Okinawa Trough which is located in the eastern of TTVG (Guo et al., 2016; Chen et al., 2018; Zhang et al., 2019; Li et al., 2020a, b; Zhang et al., 2020), indicating the subdution of Philippine Sea Plate may have same influence for these two areas.

Table 3 Trace element concentrations (ppm) of plagioclase and parental melt in TTVG

ID	Plagioclase				Partition coefficient				Parental melt							
	La	Sr	Ba	Y	La	Sr	Ba	Y	La	Sr	Ba	Y	La/Y	Sr/Y	Ba/Y	Ba/La
HRS-1	1.45	812	60.0	0.32	0.0435	1.3693	0.1281	−90	33.45	593	468	35.15	0.95	16.88	13.32	14.00
	1.77	866	79.7	0.38	0.0623	1.3775	0.1300	0.0130	28.37	629	613	29.29	0.97	21.46	20.92	21.60
	1.72	754	70.0	0.40	0.1115	1.3339	0.1198	0.0232	15.41	565	585	17.16	0.90	32.93	34.07	37.95
	1.59	863	69.0	0.31	0.0419	1.3569	0.1252	−87	37.92	636	551	35.85	1.06	17.74	15.37	14.54
	1.66	887	79.0	0.27	0.0401	1.3617	0.1263	−83	41.39	651	626	32.00	1.29	20.35	19.55	15.12
	1.38	655	38.5	0.35	0.0860	1.2760	0.1060	0.0179	16.06	513	363	19.35	0.83	26.53	18.76	22.59
	2.22	898	83.1	0.63	0.0469	1.3639	0.1268	−97	47.45	658	655	64.78	0.73	10.16	10.12	13.81
	1.97	784	73.6	0.84	0.0385	1.3462	0.1227	−80	51.14	582	600	105.07	0.49	5.54	5.71	11.73
	0.58	596	22.9	0.16	0.0454	1.3879	0.1325	−94	12.81	430	173	17.39	0.74	24.71	9.94	13.50
	1.65	776	92.7	0.33	0.1701	1.4019	0.1358	0.0354	9.70	553	683	9.37	1.04	59.05	72.92	70.45
	1.71	720	102.6	1.80	0.0880	1.3471	0.1229	0.0183	19.39	535	835	98.07	0.20	5.45	8.52	43.08
	3.44	814	90.8	2.50	0.0492	1.3722	0.1288	0.0102	69.85	593	705	243.80	0.29	2.43	2.89	10.09
	1.66	828	62.0	0.30	0.0395	1.3240	0.1174	−82	42.13	625	528	36.61	1.15	17.08	14.41	12.52
	1.65	626	46.7	0.55	0.0528	1.3761	0.1297	0.0110	31.32	455	360	50.18	0.62	9.07	7.17	11.49
	1.68	845	63.7	0.42	0.0449	1.3663	0.1247	−93	37.36	618	528	44.49	0.84	13.90	11.88	14.14
HRS-2	0.87	709	37.3	0.11	0.0251	1.2903	0.1094	−52	34.72	549	341	20.15	1.72	27.27	16.91	9.81
	1.02	731	41.9	0.15	0.0387	1.3269	0.1181	−81	26.27	551	355	18.12	1.45	30.43	19.60	13.52
	1.08	629	37.1	0.17	0.0422	1.3642	0.1269	−88	25.63	461	293	19.44	1.32	23.72	15.05	11.41
	1.68	745	42.9	0.26	0.0312	1.3033	0.1125	−65	53.79	572	381	39.57	1.36	14.44	9.64	7.09
	1.83	941	88.0	0.24	0.0410	1.3971	0.1346	−85	44.54	673	654	27.70	1.61	24.31	23.60	14.68
	0.87	732	40.2	0.13	0.0297	1.2704	0.1046	−62	29.26	576	384	20.70	1.41	27.84	18.55	13.12
	1.15	663	42.0	0.30	0.0370	1.3167	0.1157	−77	31.07	504	363	39.65	0.78	12.71	9.15	11.68
	2.77	868	84.7	1.08	0.0564	1.3819	0.1311	0.0117	49.07	628	646	92.06	0.53	6.83	7.02	13.16
	2.16	604	74.3	1.14	0.0688	1.3371	0.1205	0.0143	31.42	452	616	79.70	0.39	5.67	7.73	19.61
	0.80	649	36.8	0.13	0.0373	1.3151	0.1153	−78	21.51	494	319	17.16	1.25	28.76	18.61	14.85
	1.77	673	46.6	0.85	0.0451	1.3581	0.1255	−94	39.25	495	372	90.84	0.43	5.45	4.09	9.47
	2.76	845	129.3	0.86	0.0957	1.3682	0.1278	0.0199	28.86	618	1011	43.30	0.67	14.27	23.36	35.05
	1.60	919	73.6	0.21	0.0455	1.3538	0.1245	−95	35.15	679	591	22.37	1.57	30.34	26.43	16.82
	1.53	831	53.1	0.21	0.0276	1.3016	0.1121	−57	55.45	638	474	36.46	1.52	17.51	13.00	8.55
	1.70	822	72.2	0.37	0.0516	1.3583	0.1255	0.0107	32.98	605	575	34.31	0.96	17.65	16.76	17.43

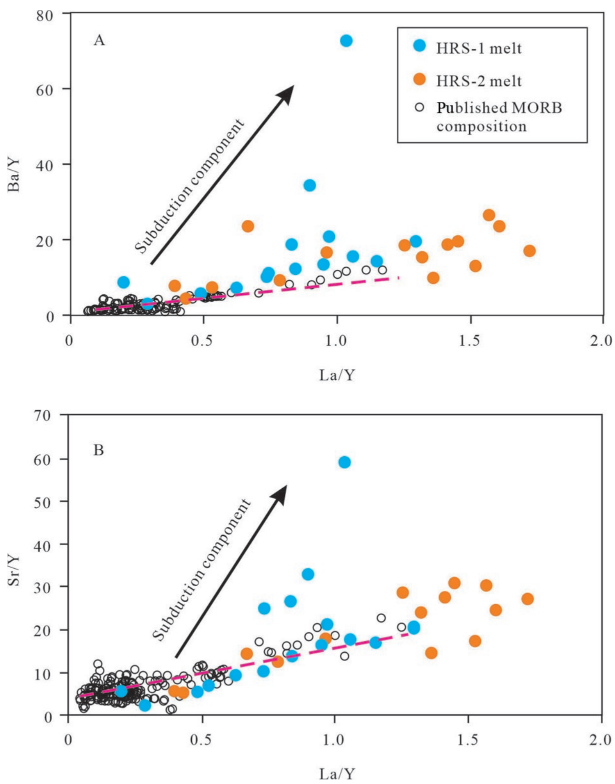

Fig. 4. Ba/Y vs. La/Y (a) and Sr/Y vs. La/Y (b) diagrams for the plagioclase parental melts in the TTVG.
The data of published MORB composition are from the Guo et al. (2018a) and reference therein.

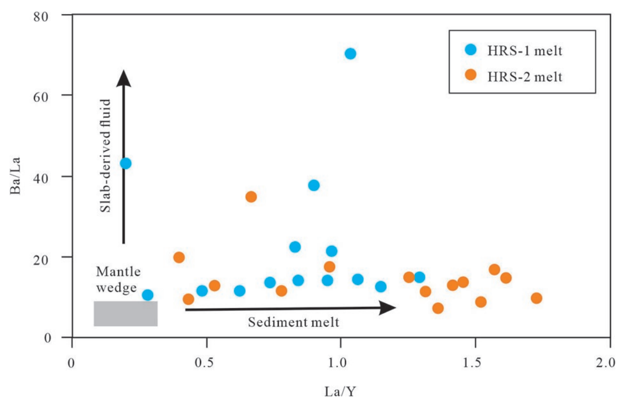

Fig. 5. Ba/Y vs. La/Y diagrams of magma melts from the TTVG.

5.2 The evolution process in mgama chamber system

A batch of magma which must go through one or numerous magma chambers may experience significant compositional and textural buffering before erupting from the subsurface (Kinman et al., 2009). And then these changes of magma would be recorded in major element zonation in textures and compositional profiles of the plagioclases that crystallized throughout crystallization evolution process (Guo et al., 2018a, b). The factors controlling the contents of elements in plagioclase are much complicated including magma mingling, magmatic evolution, melt convection and ascent-related pressure decrease (Tsuchiyama, 1985; Nelson and Montana, 1992; Chen et al., 2020), which makes the interpretation of An variation difficult. Therefore, we take the FeO concentrations of plagioclase into account during interpreting the An values variation as the influence factors of FeO contents are relatively limited (Ginibre et al., 2002).

The cores of plagioclase phenocrysts in samples HRS-1 and HRS-2 are typically coarsely sieved. This sieve-texture can be developed during the decompression process (Nelson and Montaan, 1992; Blundy and Cashman, 2001, 2005) or reaction with hotter Ca-rich melt (Tsuchiyama, 1985). In the first circumstance, the fast ascend of H_2O-undersaturated magma causes the $P(H_2O)$ of the system consequently increase, which will reduce the stability of plagioclase causing strong dissolution (Blundy and Cashman, 2001, 2005). Whereas, the reaction with a hotter Ca-rich melt results in the partial dissolution of plagioclase and generally form resorption zone and dusty zone (Tsuchiyama, 1985; Viccaro et al., 2012; Renjith, 2014). The sieve-texture caused by these two processes are quite different in size, decomposition events produce coarsely sieved texture, while superheating creates fine-size sieves (Tsuchiyama, 1985; Renjith, 2014). The cores of the plagioclase in HRS-1 and HRS-2 are coarsely sieved (Figs. 6 and 7), which may indicate that the sieved-textures are caused by the decomposition of magma system under H_2O-undersaturated condition. On the other hand, reaction with hotter Ca-rich melt usually causes the formation of reaction rim accompanied by higher An values, while the plagioclase rims in our sample have apparently lower An values than those of the cores, which further demonstrated that the coarsely sieved texture in plagioclase cores is caused by the decompression process. It is noteworthy that the cores of the plagioclase phenocrysts are much homogeneous without growth zoning, indicating that the phenocrysts' cores were crystalized in quiescent magmatic environment followed by an ascent related decompression driven dissolution (Renjith, 2014). Several synneusis are also observed in our samples (Fig. 7), which is the aggregate of two or more plagioclase. This texture is formed in a liquid-rich magma where the plagioclase crystals are bounded together by intergranular melt (Dowty, 1980; Schwindinger and Anderson, 1989; Schwindinger, 1999). Due to the synneusis has a common rim (Fig. 7), we propose that the synneusis texture was formed before the crystallization of plagioclase rim.

In several plagioclase phenocrysts' cores, weak oscillatory zoning was observed (Fig. 6c). The oscillatory zoning can be formed by changes in magma composition or physical parameters of the system (dynamic model; Panjasawatwong et al., 1995; Ginibre et al., 2002; Humphreys et al., 2006; Gevorgyan et al., 2018), which is usually resulted from the convective movements of melt in magma chamber. Alternatively, it may be ruled by the plagioclase oversaturation of the melt in relation to undercooling at the crystal-melt interface, in a way that when the system is sufficiently undercooled, at high crystal growth rate the element diffusion kinetics are too slow to re–establish the melt composition at the crystal interface (kinetic model; Pearce, 1994). Oscillatory zoning formed during the kinetic process is characterized by high frequency and straight margin (Viccaro et al., 2012; Renjith, 2014). In our samples, the oscillatory zoning texture is relatively weak and exhibits minor resorption features like curve corners (Fig. 6c) rather than straight margin, which strongly supports a dynamic model (Renjith, 2014), demonstrating the small-scale melt convection occurred in magma chamber during the crystallization of the plagioclase cores.

The rims of the TTVG plagioclase phenocrysts are generally clear without sieve-texture and the An contents in the rims are apparently lower than those of the cores (Fig. 6). Several processes may lead to the decrease in plagioclase An contents: (1) mingling with more evolved magma; (2) fast crystallization; (3) decompression of magmatic system under H_2O-saturated condition (Viccaro et al., 2010; Renjith, 2014; Lai et al., 2016). Both of mingling with more evolved magma and fast crystallization of plagioclase will cause the decrease in An and FeO contents simultaneously (e.g., Lai et al, 2016; Chen et al., 2020). However, the FeO concentrations in the rims of the plagioclase phenocrysts are apparently higher compared with the core, which cannot be explained by the processes 1 and 2. As we mentioned above, ascent related decompression of magma system under H_2O-undersaturated condition causes the strongly dissolution of plagioclase. While if H_2O-saturation is reached, water will lose from the system causing the crystallization of more sodic plagioclase rim (lower An contents; Viccaro et al., 2010). Thus, we propose that decompression of magmatic system under H_2O-saturated condition is the major cause for An contents decrease in the plagioclase rim. During the ascent of melt (decompression process), the fO_2 increase gradually. As the Fe partitioning between plagioclase and melt is positively correlated with fO_2 (Phinney et al., 1992; Bindeman et al., 1998; Wilke and Behrens, 1999; Humphreys et al., 2006, 2009), the FeO contents in the plagioclase rim increase in response to elevated fO_2.

The textures and chemical composition (Figs. 2 and 6) of plagioclase cores and rims are quite different, which implies that the cores and rims of the plagioclase phenocrysts in TTVG were crystalized in different physicochemical conditions. We propose that there may exist double-layer magma chamber system in TTVG. The homogeneous core was crystalized in the deeper quiescent magma chamber. During the ascent of the magma, the pressure of system decreases gradually causing the dissolution of early crystalized plagioclase under H_2O-undersatuated condition. The H_2O contents and fO_2 may be relatively higher in the shallower chamber. When magma melt migrates to the shallower chamber, the water saturation reached and more sodic plagioclase formed as the rim of phenocryst. Meanwhile, increase in fO_2 causes the stronger substitution of Fe into plagioclase, resulting in the elevated FeO contents in the rim. The thickness of the plagioclase rim falls between 20–50 μm, according to the growth rates of plagioclase in basaltic magmatic system (~10^{-10}cm/s; Marsh, 1988; Cashman and Marsh, 1988; Cashman, 1988, 1990, 1992), the magma melt stayed in the shallow chamber for about 7–15 months before eruption.

5.3 Temperature and depth of magma chamber

Previous researches have demonstrated that plagioclase-

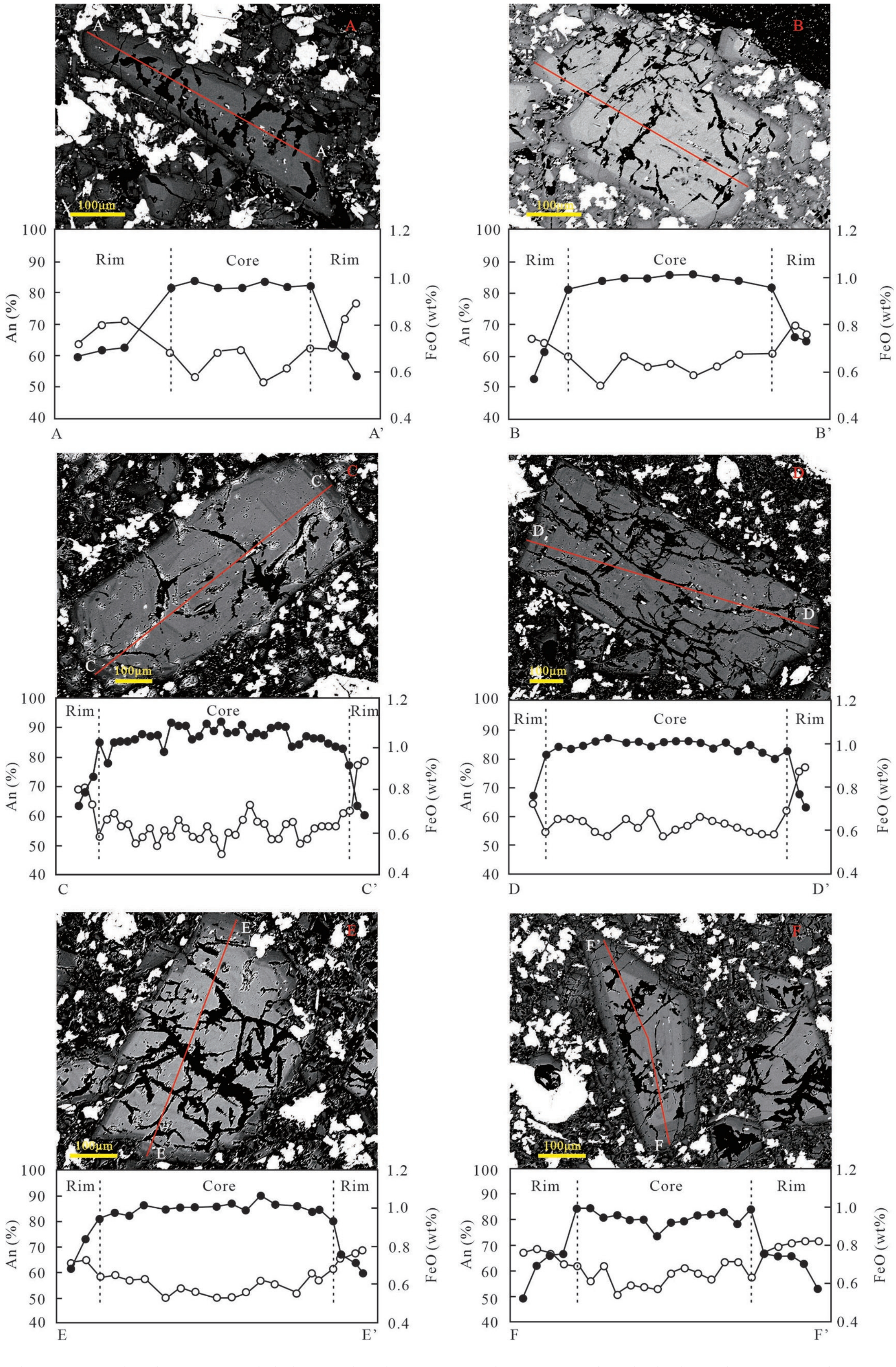

Fig. 6. Example of textures and their associated An-FeO zoning patterns for plagioclase phenocrysts of TTVG volcanic rocks.

a–c: grain 1, 2, 3 in HRS-1; d–f: grain 1, 2, 3 in HRS-2. Filled circles: An%; open circles: FeO wt%.

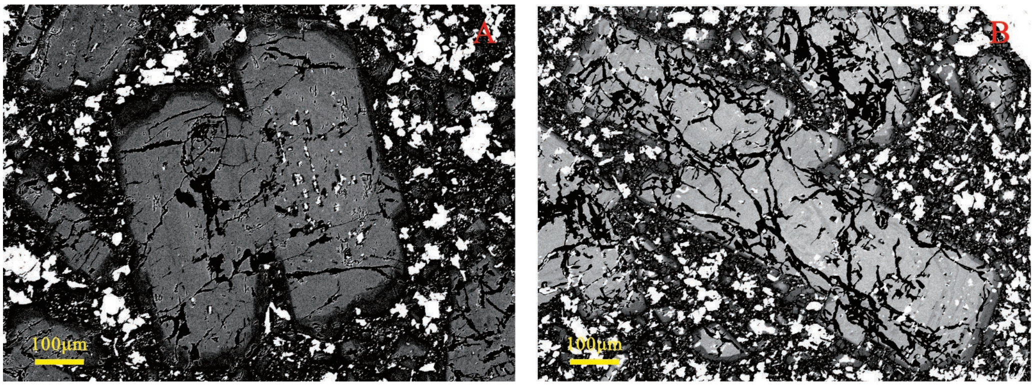

Fig.7. Synneusis of plagioclase grains in (a) HRS-1 and (b) HRS-1.
The coarsely sieved plagiocalses interlocked together and developed a common clear rim.

melt equilibrium can be used to calculate the crystallization temperature and pressure of plagioclase (Ghiorso and Sack, 1995; Sugawara, 2001; Ghiorso et al., 2002; Putirka, 2005, 2008), which has been widely applied to estimate the depth and temperature of magma chamber (e.g., Guo et al., 2018a). As we mentioned in section 5.2, there exists double–layer chamber in TTVG magma system. The core of plagioclase was formed in the deeper chamber, while the plagioclase rim was crystalized after melt ascending to the shallower chamber. In order to estimate the temperature and depth of the magma chambers, we attempt to calculate the crystallization temperature and pressure of plagioclase core and rim respectively according to the thermobarometry model proposed by Putirka (2008), where the melt composition was represented by average whole rock composition of TTVG basalts. Most of the $K_D(Ab–An)^{pl–liq}$ values of the plagioclase core are within 0.27 ± 0.11, indicating that the core of plagioclase was in equilibrium with their whole rock composition (Fig. 8). Those data fall in the equilibrium range were used to do the thermobarometry calculation and results show that the crystallization temperature and pressure of plagioclase core are ~1245 °C and ~8 kbar respectively, indicating that the depth of deeper magma chamber is about 21 km (ρ_{crust} = 2.7 g/cm^3; Telford et al., 1990). While the rim of plagioclase was not in equilibrium with the whole rock composition, thus, the calculated results do not represent the correct crystallization temperature and pressure for the plagioclase rim.

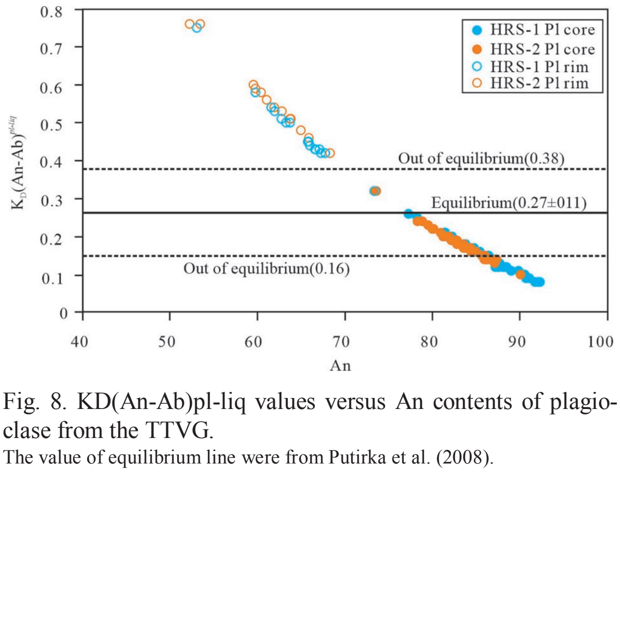

Fig. 8. KD(An-Ab)pl-liq values versus An contents of plagioclase from the TTVG.
The value of equilibrium line were from Putirka et al. (2008).

5.4 Dynamics of magmatic system

The detailed study of plagioclase textural and compositional features provides valuable information on the dynamics of TTVG magmatic systems. The TTVG volcanic rocks studied in this paper were formed after westward propagation of the Philippine Sea Plate under the Northern Taiwan. The magma melts are mainly sourced from the underlying mantle wedge, meanwhile, subduction of the Philippine Sea Plate causing the incorporation of slab-derived material into the magma source (Fig. 9a), resulting in the elevated Sr/Y and Ba/Y ratios in the magma melts. The subduction components are mainly transported in the form of sediment melt with little proportion of slab-derived aqueous fluid.

There exists double-layer magma chamber in the TTVG magmatic system. The lower chamber is located in the depth of ~21 km and the temperature of the magma melt is about 1245°C. Magmatic environment in this chamber is relatively quiescent, resulting in the crystallization of homogeneous plagioclase (Fig. 9b). Meanwhile, several weak zoning plagioclase phenocrysts indicate small scale melt convection might occurred during the magmatic process. During the ascent of this crystal-rich melt to the shallower magma chamber, strong dissolution of the plagioclase occurred due to the decompression under H_2O-undersaturated condition, causing the formation of coarse-sieve texture (Fig. 9b). In this process, two or more plagioclase phenocrysts are binding together by the intergranular melt forming the so-called synneusis texture. The H_2O contents and fO_2 was relatively higher in the shallower chamber. When magma melt migrated to the shallower chamber, the water saturation reached and more sodic plagioclase formed as the rim of phenocryst, the An contents of the plagioclase rim sharply drop as a result. Due to the fO_2 in the shallower chamber is higher than that of the deeper chamber and the Fe partitioning between plagioclase and melt is positively correlated with fO_2 (Phinney et al., 1992; Bindeman et al., 1998; Wilke and Behrens, 1999; Humphreys et al., 2006, 2009), the FeO contents in the plagioclase rim elevate as a result of fO_2

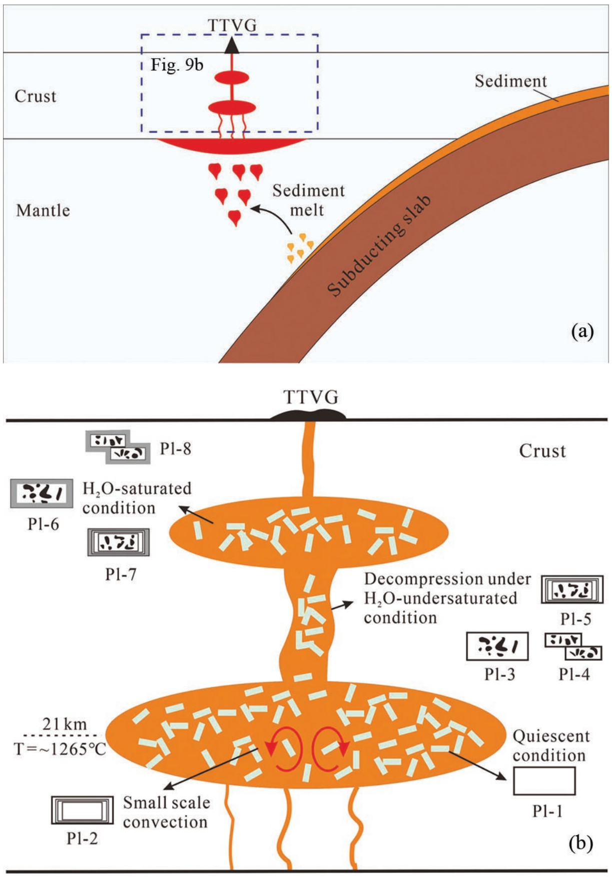

Fig.9. Dynamics of magmatic system at Tatun Volcanic Group.
Pl-1: homogeneous plagioclase; Pl-2: weak zoning plagioclase; Pl-3: core-sieved plagioclase; Pl-4: synneusis; Pl-5: core-sieved weak zoning plagioclase; Pl-6, Pl-7, Pl-8: core-sieved plagioclase with clear rim. Graph not to scale.

increase. After 7–15 months, the crystal-rich magma erupted from the shallower chamber and condensed as basalt.

This paper conducted systematic research of textural and compositional characteristics of plagioclase from the TTVG volcanic rocks, on this basis, the magma source compositions and magmatic process were discussed, which is of great significance for deepening us understanding of petrogenesis of mafic magma in post-collisional settings. Meanwhile, this research is beneficial to better understand the variation of geochemical composition of magma in the whole process from collision to cessation.

6 Conclusion

(1) The magma melts in TTVG are mainly sourced from the underlying MORB-like mantle wedge but influenced by incorporation of subduction components and the subduction components are mainly transported in the form of sediment melt.

(2) The plagioclase phenocrysts in the TTVG volcanic rocks generally have coarsely sieved core and a clear rim, the An contents in the rims of plagioclase are much lower than those of cores, and elevated FeO concentrations are detected in the plagioclase rims. A double-layer magma chamber is proposed in TTVG. The core of plagioclase was crystalized in the deeper quiescent magma chamber and subsequently partially dissolved during the ascent of magma melt under H_2O-undersaturation condition. When magma migrated into the shallower chamber, the water saturation reached and more sodic plagioclase formed as the rim of phenocryst. Meanwhile, increase in fO_2 in shallower magma chamber causes the elevated FeO contents in the plagioclase rim.

Acknowledgments

We thank Dr. Pi Ju-lien for collecting the samples. We acknowledge Dr. Hripsime Gevorgyan and an anonymous reviewer for their constructive comments on the earlier version of this manuscript. This work was funded by the Shandong Provincial Natural Science Foundation, China (No. ZR2019BD010), the National Natural Science Foundation of China (No. 42276085), Open Fund of the Key Laboratory of Marine Geology and Environment, Chinese Academy of Sciences (No. MGE2021KG01), Pilot National Laboratory for Marine Science and Technology (Qingdao) (No. JCZX202014) and the Key Laboratory Submarine Geoscience and Prospecting Techniques, Ministry of Education, Ocean university of China.

Manuscript received May 21, 2021
accepted Sep. 08, 2021
associate EIC: XU Jifeng
edited by FEI Hongcai

Supplementary material to this article can be found online at https://doi.org/10.1111/1755-6724.14810.

References

Bindeman, I.N., Davis, A.M., and Drake, M.J., 1998. Ion microprobe study of plagioclase-basalt partition experiments at natural concentration level of trace elements. Geochimica et Cosmochimica Acta, 62: 660–676.

Blundy, J.D., and Shimizu, N., 1991. Trace element evidence for plagioclase recycling in calc–alkaline magmas. Earth and Planetary Science Letters, 102: 178–197.

Blundy, J., and Cashman, K., 2001. Ascent-driven crystallization of dacite magmas at Mount St. Helens, 1980–1986. Contributions to Mineralogy and Petrology, 140: 631–650.

Blundy, J., and Cashman, K., 2005. Rapid decompression-driven crystallization recorded by melt inclusions from Mount St. Helens Volcano. Geology, 33: 793–796.

Cashman, K.V., and Marsh, B.D., 1988. Crystal size distribution (CSD) in rocks and the kinetics and dynamics of crystallization II: Makaopuhi lava lake. Contributions to Mineralogy and Petrology, 99: 292–305.

Cashman, K.V., 1988. Crystallisation of Mount St. Helens 1980–1986 dacite: A quantitative textural approach. Bulletin of Volcanology, 50: 194–209.

Cashman, K.V., 1990. Textural constraints on the kinetics of crystallization of igneous rocks. In: Nicholls, J., and Russell, J.K. (eds.), Modern Methods of Igneous Petrology, Understanding Magmatic Process: Reviews in Mineralogy. Mineralogical Society of America, Washington, D.C.

Cashman, K.V., 1992. Groundmass crystallization of Mount St. Helens dacite 1980–1986: A tool for interpreting shallow magmatic processes. Contributions to Mineralogy and Petrology, 109: 431–449.

Chen, C.H., 1997. Extensional collapse of the northern Taiwan

mountain belt: comment. Geology, 25: 855–856.
Chen, Z., Zeng, Z., Wang, X., Yin, X., Chen, S., Guo, K., Lai, Z., Zhang, Y., Ma, Y., Qi, H., and Wu, L., 2018. U-Th/He dating and chemical compositions of apatite in the dacite from the southwestern Okinawa Trough: Implications for petrogenesis. Journal of Asian Earth Sciences, 161: 1–13.
Chen, Z., Zeng, Z., Wang, X., Peng, X., Zhang, Y., Yin, X., Chen, S., Zhang, L., and Qi, H., 2020. Element and Sr isotope zoning in plagioclase in the dacites from the southwestern Okinawa Trough: Insights into magma mixing processes and time scales. Lithos, 376–377: 105776.
Chung, S., Yang, T., Lee, C., and Chen, C., 1995. The igneous provinciality in Taiwan: consequence of continental rifting superimposed by Luzon and Ryukyu subduction systems. Journal of Asian Earth Sciences, 11: 73–80.
Chung, S., Chu, M., Zhang, Y., Xie, Y., Lo, C., Lee, T., Lan, C., Li, X., Zhang, Q., and Wang, Y., 2005. Tibetan tectonic evolution inferred from spatial and temporal variations in post -collisional magmatism. Earth-Science Reviews, 68: 173–196.
Dai, F., Zhao, Z., Dai, L., and Zheng, Y., 2016. Slab-mantle interaction in the petrogenesis of andesitic magmas: Geochemical evidence from postcollisional intermediate volcanic rocks in the Dabie Orogen, China. Journal of Petrology, 57(6): 1109–1134.
Dong, Y., Zhang, G., Neubauer, F., Liu, X., Hauzenberger, C., Zhou, D., and Li, W., 2011. Syn- and post-collisional granitoids in the Central Tianshan orogen: Geochemistry, geochronology and implications for tectonic evolution. Gondwana Research, 20: 568–581.
Dowty, E., 1980. Synneusis reconsidered. Contributions to Mineralogy and Petrology, 74: 75–84.
Gao, P., Zhao, Z., and Zheng, Y., 2014. Petrogenesis of Triassic granites from the Nanling Range in South China: Implications for geochemical diversity in granites. Lithos, 210–211: 40–56.
Gevorgyan, H., Repstock, A., Schulz, B., Meliksetian, K., Breitkreuz, C., and Israyelyan, A., 2018. Decoding a post-collisional multistage magma system: The Quaternary ignimbrites of Aragats stratovolcano, western Armenia. Lithos, 318: 267–282.
Ghiorso, M.S., and Sack, R.O., 1995. Chemical mass transfer in magmatic processes IV. A revised and internally consistent thermodynamic model for the interpolation and extrapolation of liquid-solid equilibria in magmatic systems at elevated temperatures and pressures. Contributions to Mineralogy and Petrology, 119: 197–212.
Ghiorso, M.S., Hirschmann, M.M., Reiners, P.W., and Kress, V.C. III., 2002. The pMELTS: A revision of MELTS for improved calculation of phase relations and major element partitioning related to partial melting of the mantle to 3 GPa. Geochemistry Geophysics Geosystems, 3: 1–36.
Gill, J.B., 1981. Orogenic andesites and plate tectonics. Berlin: Springer, 1–390.
Ginibre, C., Kronz, A., and Wörner, G., 2002. High-resolution quantitative imaging of plagioclase composition using accumulated backscattered electron images: New constraints on oscillatory zoning. Contributions to Mineralogy and Petrology, 142: 436–448.
Grove, T.L., Baker, M.B., and Kinzler, R.J., 1984. Coupled CaAl -NaSi diffusion in plagioclase feldspar: Experiments and applications to cooling rate speedometry. Geochemica et Cosmochimica Acta, 48: 2113–2121.
Guo, K., Zhai, S.K., Yu, Z.H., Cai, Z.W., and Zhang, X., 2016. Sr-Nd-Pb isotopic geochemistry of phenocrysts in pumice from the central Okinawa Trough. Geological Journal, 51: 368 –375.
Guo, K., Zhai, S.K., Wang, X.Y., Yu, Z.H., Lai, Z.Q., Chen, S., Zhao, J.S., Ma, Y., Chen, Z.X., and Li, X.H., 2018a. The dynamics of the southern Okinawa Trough magmatic system: New insights from the microanalysis of An contents, trace element concentrations and Sr isotopic compositions of plagioclase hosted in basalts and acid rocks. Chemical Geology, 497: 146–161.
Guo, K., Zhai, S., Yu, Z., Wang, S., Zhang, X., and Wang, X., 2018b. Geochemical and Sr–Nd–Pb–Li isotopic characteristics of volcanic rocks from the Okinawa Trough: Implications for the influence of subduction components and the contamination of crustal materials. Journal of Marine Systems, 180: 140–151.
Hébert, R., Guilmette, C., Dostal, J., Bezard, R., Lesage, G., Bédard, E., and Wang, C., 2014. Miocene post–collisional shoshonites and their crustal xenoliths, Yarlung Zangbo Suture Zone southern Tibet: Geodynamic implications. Gondwana Research, 25: 1263–1271.
Hu, Y., Niu, Y., Li, J., Ye, L., Kong, J., Chen, S., Zhang, Y., and Zhang, G., 2016. Petrogenesis and tectonic significance of the late Triassic mafic dikes and felsic volcanic rocks in the East Kunlun Orogenic Belt, Northern Tibet Plateau. Lithos, 245: 205–222.
Huang, P., Song, C., Xiao, W., Li, J., Zhou, K., Wang, J., Abuduxun, N., and Li, Z., 2021. Deformation and geochronology of the Xiaotian–Mozitan shear zone in the Dabie Orogenic Belt (East–Central China), and their geological significance. Acta Geologica Sinica (English Edition), 95(1): 370–392.
Humphreys, M.C.S., Blundy, J.D., and Sparks, S.J., 2006. Magma evolution and open system processes at Shiveluch volcano: Insights from phenocryst zoning. Journal of Petrology, 47: 2303–2334.
Humphreys, M.C.S., Christopher, T., and Hards, V., 2009. Microlite transfer by disaggregation of mafic inclusions following magma mixing at Soufrière Hills volcano, Montserrat. Contributions to Mineralogy and Petrology, 157: 609–624.
Kinman, W.S., Neal, C.R., Davidson, J.P., and Font, L., 2009. The dynamics of Kerguelen Plateau magma evolution: New insights from major element, trace element and Sr isotope microanalysis of plagioclase hosted in Elan Bank basalts. Chemical Geology, 264: 247–256.
Kong, J., Niu, Y., Hu, Y., Zhang, Y., and Shao, F., 2020. Petrogenesis of the triassic granitoids from the East Kunlun Orogenic Belt, NW China: Implications for continental crust growth from syncollisional to post-collisional setting. Lithos, 364–365: 105513.
Lai, Z., Zhao, G., Han, Z., Liu, B., Bu, X., and Leng, C., 2016. Back-arc magma processes in the Okinawa Trough: New insights from textural and compositional variations of plagioclase in basalts. Geological Journal, S1: 346–356.
Lai, Z., Zhao, G., Han, Z., Huang, B., Li, M., Tian, L., Liu, B., and Bu, X., 2018. The magma plumbing system in the Mariana Trough back-arc basin at 18° N. Journal of Marine Systems, 180: 132–139.
Laurent, A., Janousek, V., Magna, T., Schulmann, K., and Míková, J., 2015. Petrogenesis and geochronology of a post-orogenic calc-alkaline magmatic association: The Zulová Pluton, Bohemian Massif. Journal of Geosciences, 59: 415–440.
Li, X., Zeng, Z., Dan, W., Yang, H., Wang, X., Fang, B., and Li, Q., 2020a. Source lithology and crustal assimilation recorded in low δ^{18}O olivine from Okinawa Trough, back-arc basin. Lithos, 360–361: 105444.
Li, X., Zeng, Z., Yang, H., Zhao, Y., Yin, X., Wang, X., Chen, S., Qi, H., and Guo, K., 2020b. Integrated major and trace element study of clinopyroxene in basic, intermediate and acidic volcanic rocks fromthemiddle Okinawa Trough: Insights into petrogenesis and the influence of subduction component. Lithos, 352: 105320.
Li, Y., Xiao, W., Zheng, J., and Brouwer, F.M., 2022. Northward subduction of the South Qilian ocean: Insights from early Paleozoic magmatism in the south-central Qilian belts. Geosystems and Geoenvironment, 1: 100013.
Liu, D., Zhao, Z., Zhu, D., Niu, Y., De Paolo, D.J., Harrison, T.M., Mo, X., Dong, G., Zhou, S., Sun, C., Zhang, Z., and Liu, J., 2014. Postcollisional potassic and ultrapotassic rocks in Southern Tibet: Mantle and crustal origins in response to india–asia collision and convergence. Geochimica et Cosmochimica Acta, 143: 207–231.
Liu, Y., Hu, Z., Zong, K., Gao, C., Gao, S., Xu, J., and Chen, H., 2010. Reappraisement and refinement of zircon U-Pb isotope and trace element analyses by LA-ICP-MS. Chinese Science Bulletin, 55: 1535–1546.

Manikyamba, C., Pahari, A., Santosh, M., Subramanyam, K.S.V., and Reddy, G.H., 2022. Geochemistry of basalts in unravelling the mantle processes and crustal evolution: Insights from the greenstone belts of western Dharwar Craton. Geosystems and Geoenvironment, 1: 100070.

Marsh, B.D., 1988. Crystal size distribution (CSD) in rocks and the kinetics and dynamics of crystallisation I. Theory. Contributions to Mineralogy and Petrology, 99: 277–291.

Meshram, T., Mahapatro, S., Sesha Sai, V.V., Dora, M.L., Randive, K., and Baswani, S., 2022. Petrogenesis of phlogopite-pyroxenite from Southern India: Implications for the link between Proterozoic subduction- to rift-related arc magmatism. Geosystems and Geoenvironment, 1: 100033.

Nelson, S.T., and Montana, A., 1992. Sieve-textured plagioclase in volcanic rocks produced by rapid decompression. American Mineralogist, 77: 1242–1249.

Panjasawatwong, Y., Danyushevsky, L., Crawford, A., and Harris, K., 1995. An experimental study of the effects of melt composition on plagioclase-melt equilibria at 5–kbar and 10–kbar–Implications for the origin of magmatic high-An plagioclase. Contributions to Mineralogy and Petrology, 118 (4): 420–432.

Pearce, T.H., 1994. Recent work on oscillatory zoning in plagioclase. In: Parsons (ed.), Feldspars and Their Reactions. NATO ASI Series, Series C: Mathematical and Physical Sciences 421. Kluwer Academic Publication, 313–349.

Pearce, J.A., Bender, J.F., De Long, S.E., Kidd, W.S.F., Low, P.J., Guner, Y., Saroglu, F., Yilmaz, Y., Moorbath, S., and Mitchell, J.G., 1990. Genesis of collision volcanism in Eastern Anatolia, Turkey. Journal of Volcanology and Geothermal Research, 44: 189–229.

Phinney, W.C., 1992. Partitioning coefficients for ion between plagioclase and basalt as a function of oxygen fugacity: Implications for Archean and lunar anorthosites. Geochimica et Cosmochimica Acta, 56: 1885–1895.

Pi, J., You, C., and Wang, K., 2016. The influence of Ryukyu subduction on magma genesis in the Northern Taiwan Volcanic Zone and Middle Okinawa Trough—Evidence from boron isotopes. Lithos, 260: 242–252.

Putirka, K.D., 2005. Igneous thermometers and barometers based on plagioclase+liquid equilibria: Tests of some existing models and new calibrations. American Mineralogist, 90: 336–346.

Putirka, K.D., 2008. Thermometers and barometers for volcanic systems. Reviews in Mineralogy & Geochemistry. 69: 61–120.

Rateb, A., Ching, K.E., Kuo, C.Y., Rau, R.J., and Chen, C.L., 2017. Kinematics of the tectonic blocks and active faults at the post-orogenic stage: Northern Taiwan. Journal of Asian Earth Sciences, 149: 29–40.

Renjith, M.L., 2014. Micro-textures in plagioclase from 1994–1995 eruption, Barren Island Volcano: Evidence of dynamic magma plumbing system in the Andaman subduction zone. Geoscience Frontiers, 5: 113–126.

Schwindinger, K.R., and Anderson Jr., A.T., 1989. Synneusis of Kilauea Iki olivines. Contributions to Mineralogy and Petrology, 103: 187–198.

Schwindinger, K.R., 1999. Particle dynamics and aggregation of crystals in a magma chamber with application to Kilauea Iki olivines. Journal of Volcanology and Geothermal Research, 88: 209–238.

Seghedi, I., Besutiu, L., Mirea, V., Zlagnean, L., Popa, R., Szakács, A., Atanasiu, L., Pomeran, M., and Vişan, M., 2019. Tectono-magmatic characteristics of post-collisional magmatism: Case study East Carpathians, Călimani–Gurghiu–Harghita volcanic range. Physics of the Earth and Planetary Interiors. 293: 106270.

Singer, B.S., Dungan, M.A., and Layn, G.D., 1995. Textures and Sr, Ba, Mg, Fe, K, and Ti compositional profiles in volcanic plagioclase: Clues to the dynamics of calcalkaline magma chambers. American Mineralogist, 80: 776–798.

Smith, V.C., Blundy, J.D., and Arce, J.L., 2009. Temporal record of magma accumulation and evolution beneath Nevado de Toluca, Mexico, preserved in plagioclase phenocrysts. Journal of Petrology, 50: 405–426.

Stimac, J.A., and Pearce, T.H., 1992. Textural evidence of mafic-feslic magma interaction in dacite lavas, Clear Lake, California. American Mineralogist, 77: 795–809.

Sugawara, T., 2001. Ferric iron partitioning between plagioclase and silicate liquid: Thermodynamics and petrological applications. Contributions to Mineralogy and Petrology, 141 (6): 659–686.

Sun, S.S., Mcdonough, W.F., 1989. Chemical and isotopic systematics of oceanic basalts: implications for mantle composition and processes. Special Publication Geological Society of London, 42: 313–345.

Sun, C., Graff, M., and Liang, Y., 2017. Trace element partitioning between plagioclase and silicate melt: the importance of temperature and plagioclase composition, with implications for terrestrial and lunar magmatism. Geochimica et Cosmochimica Acta, 206: 273–295.

Telford, W.N., Geldart, L.P., Sheriff, R.E., and Keys, D.A., 1990. Applied geophysics. Cambridge: Cambridge University Press.

Teng, L.S., 1996. Extensional collapse of the northern Taiwan mountain belt. Geology, 24: 949–952.

Tepley III, F.J., Davidson, J.P., Tilling, R.I., and Arth, J.G., 2000. Magma mixing, recharge and eruption histories recorded in plagioclase phenocrysts from El Chichón volcano, Mexico. Journal of Petrology, 41: 1397–1411.

Tian, Z., Yan, Y., Huang, C., Zhang, X., Liu, H., Yu, M., Yao, D., and Dilek, Y., 2019. Geochemistry and geochronology of the accreted mafic rocks from the Hengchun Peninsula, southern Taiwan: Origin and tectonic implications. Journal of Geophysical Research: Solid Earth, 124(3): 2469–2491.

Tsuchiyama, A., 1985. Dissolution kinetics of plagioclase in the melt of the system diopside–albite–anorthite, and origin of dusty plagioclase in andesites. Contributions to Mineralogy and Petrology, 89: 1–16.

Turner, S., Arnaud, N., Liu, J., Rogers, N., Hawkesworth, C., Harris, N., Kelley, S., Calsteren, P.V., and Deng, W., 1996. Post-collision, shoshonitic volcanism on the Tibetan plateau: Implications for convective thinning of the lithosphere and the source of ocean island basalts. Journal of Petrology, 1: 45–71.

Viccaro, M., Giacomoni, P.P., Ferlito, C., Cristofolini, R., 2010. Dynamics of magma supply at Mt. Etna volcano (Southern Italy) as revealed by textural and compositional features of plagioclase phenocrysts. Lithos, 116: 77–91.

Viccaro, M., Giuffridaa, M., Nicotraa, E., and Ozerov, Y.A., 2012. Magma storage, ascent and recharge history prior to the 1991 eruption at Avachinsky Volcano, Kamchatka, Russia: Inferences on the plumbing system geometry. Lithos, 140–141: 11–24.

Wang, K., Chung, S., O'Reilly, S.Y., Sun, S., Shinjo, R., and Chen, C., 2004. Geochemical constraints for the genesis of post-collisional magmatism and the geodynamic evolution of the northern Taiwan Region. Journal of Petrology, 45: 975–1011.

Wang, K.L., Chung, S.L., Shinjo, R., Chen, C.H., Yang, T.F., and Chen, C.H., 1999. Post collisional magmatism around northern Taiwan and its relation with opening of the Okinawa Trough. Tectonophysics, 308: 363–376.

Wang, S., and Zhang, G., 2022. Geochemical constraints on mantle source nature and recycling of subducted sediments in the Sulu Sea. Geosystems and Geoenvironment, 1: 100005.

Wilke, M., and Behrens, H., 1999. The dependence of partitioning of iron and europium between plagioclase and hydrous tonalitic melt on oxygen fugacity. Contributions to Mineralogy and Petrology, 137: 102–114.

Zhang, K., Wang, J., He, W., Wang, S., Xu Y., Zhang, X., Song, B., Kou X., and Wang, G., 2022. Reconstructed ocean plate stratigraphy sequences from the Permian subduction-accretionary complex in the Qinghai-Tibet Plateau. Geosystems and Geoenvironment, 1: 100034.

Zhang, X., Zhai, S., Yu, Z., Guo, K., and Wang, S., 2019. Subduction contribution to the magma source of the Okinawa Trough–Evidence from boron isotopes. Geological Journal, 54: 605–613.

Zhang, Y., Zeng, Z., Gaetani, G., Zhang, L., and Lai, Z., 2020. Mineralogical constraints on the magma mixing beneath the

Iheya Graben, an active back-arc spreading center of the Okinawa Trough. Journal of Petrology, DOI: 10.1093/petrology/egaa098.

Zhao, Z., Zheng, Y., Wei, C., and Wu, F., 2011. Origin of postcollisional magmatic rocks in the Dabie orogen: Implications for crust–mantle interaction and crustal architecture. Lithos, 126: 99–114.

Zhao, Z., Dai, L., and Zheng, Y., 2013. Postcollisional mafic igneous rocks record crust-mantle interaction during continental deep subduction. Scientific Reports, 3: 3413.

Zhao, Z., Gao, P., and Zheng, Y. F., 2015. The source of Mesozoic granitoids in South China: Integrated geochemical constraints from the Taoshan batholith in the Nanling Range. Chemical Geology, 395: 11–26.

Zheng, Y., Xia, Q., Chen, R., and Gao, X., 2011. Partial melting, fluid supercriticality and element mobility in ultrahigh-pressure metamorphic rocks during continental collision. Earth–Science Reviews, 107: 342–374.

Zheng, Y., Chen, Y., Dai, L.Q., and Zhao, Z., 2015. Developing plate tectonics theory from oceanic subduction zones to collisional orogens. Science China: Earth Science, 58: 1045–1069.

About the first author

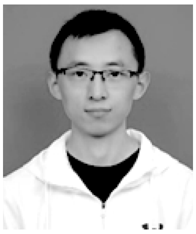

ZHANG Xia, male, born in 1991 in Jinzhong, Shanxi Province; doctor; graduated from Ocean University of China; research assistant of Qingdao National Laboratory of Marine Science and Technology. He is now interested in the study on modern seafloor hydrothermal mineralization and magmatic process. E-mail: xzhang4@qnlm.ac.

About the corresponding author

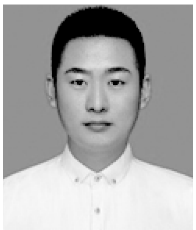

GUO Kun, male, born in 1986 in Qingdao, Shandong Province; doctor; graduated from Ocean University of China; senior engineer of Qingdao National Laboratory of Marine Science and Technology. He is now interested in the study on magmatism and magma chamber process of subduction, and isotope analysis method of TIMS. E-mail: kguo@qnlm.ac.